scientific reports

Check for updates

OPEN

Exploring adsorption capacity and mechanisms involved in cadmium removal from aqueous solutions by biochar derived from euhalophyte

Shaoqing Ge[1], Shuai Zhao[1]✉, Lei Wang[1], Zhenyong Zhao[1], Shoule Wang[1,2] & Changyan Tian[1]✉

Biochar has shown potential as a sorbent for reducing Cd levels in water. Euhalophytes, which thrive in saline-alkali soils containing high concentrations of metal ions and anions, present an intriguing opportunity for producing biochar with inherent metal adsorption properties. This study focused on biochar derived from the euhalophyte *Salicornia europaea* and aimed to investigate its Cd adsorption capacity through adsorption kinetics and isotherm experiments. The results demonstrated that *S. europaea* biochar exhibited a high specific surface area, substantial base cation content, and a low negative surface charge, making it a highly effective adsorbent for Cd. The adsorption data fit well with the Langmuir isotherm model, revealing a maximum adsorption capacity of 108.54 mg g^{-1} at 25 °C. The adsorption process involved both surface adsorption and intraparticle diffusion. The Cd adsorption mechanism on the biochar encompassed precipitation, ion exchange, functional group complexation, and cation-π interactions. Notably, the precipitation of Cd^{2+} with CO_3^{2-} in the biochar played a dominant role, accounting for 73.7% of the overall removal mechanism. These findings underscore the potential of euhalophytes such as *S. europaea* as a promising solution for remediating Cd contamination in aquatic environments.

Cadmium (Cd) is a highly prevalent metal pollutant in water, presenting significant risks to both ecological and human health due to its high biological toxicity, mobility, and potential for accumulation[1]. According to the U.S. Environmental Protection Agency (EPA), the maximum allowable level of cadmium in drinking water is 0.005 mg per liter[2]. Various techniques are available for removing Cd from wastewater, including solvent extraction, chemical precipitation, membrane filtration, electrochemical methods and adsorption[3–5]. Considering various techniques, the adsorption of Cd using adsorbents is an economically viable method for remediating contaminated water[6].

Biochar, derived from biomass (such as plant residues, agricultural waste, and manure) through pyrolysis under oxygen-limited conditions, is a carbon-rich byproduct. It serves as a widely used, cost-effective adsorbent for various pollutants in aqueous solutions[7,8]. The mechanism of of Cd^{2+} adsorption on biochar has been undertaken to studied extensively, uncovering several key processes: (1) Precipitation involving minerals present in biochar, such as CO_3^{2-}, OH^-, PO_4^{3-}, and SO_4^{2-}[9–11]. (2) Exchange of Cd^{2+} with other metal ions, such as Ca^{2+}, Mg^{2+}, K^+, Na^+, and –COOM[12]. (3) Surface complexation with oxygen-containing functional groups, such as –OH and –COOH[13]. (4) Cation-π interactions involving aromatic systems, C=C, and C=O[14,15]. These investigations have provided valuable insights into the diverse mechanisms underlying Cd^{2+} adsorption onto biochar, highlighting the complex nature of the adsorption process.

The adsorption capacity of biochar for Cd^{2+} has demonstrated limitations in prior tests. For instance, biochars derived from maize stalks (pyrolyzed at 500 °C) and rapeseed straw (pyrolyzed at 600 °C) exhibited Cd^{2+} adsorption capacities of 12.67 mg g^{-1} and 32.74 mg g^{-1}, respectively[16,17]. Similarly, livestock manure-derived biochar (pyrolyzed at 450 °C) demonstrated a Cd^{2+} adsorption capacity of 8.89 mg g^{-1}[18]. The constrained adsorption

[1]State Key Laboratory of Desert and Oasis Ecology, Xinjiang Institute of Ecology and Geography, Chinese Academy of Sciences, 818 South Beijing Road, Ürümqi 830011, Xinjiang, China. [2]Shandong Institute of Pomology, Taian 271000, China. ✉email: zhaoshuai@ms.xjb.ac.cn; tianchy@ms.xjb.ac.cn

capacity of these biochars for heavy metals is frequently attributed to their insufficient mineral content[19]. Consequently, biochar is often subjected to modifications to boost its mineral content, thereby creating more binding sites on its surface and enhancing its adsorption capacity for Cd[20,21]. Notably, recent studies have discovered that biochar pyrolyzed from euhalophytes naturally contains a substantial amount of mineral content and functional group[22,23], This revelation implies the potential of biochar from euhalophyte as an efficient Cd adsorbent. However, our comprehension of the adsorption capacity of biochar derived from euhalophyte is still in its early stage.

Euhalophytes, which can complete their life cycle in saline soils, produce substantial biomass in areas where glycophytes cannot thrive[24]. *Salicornia europaea*, a leaf succulent annual euhalophyte, is widely found in saltmarshes and mudflats worldwide. It exhibits a remarkable ability to accumulate high quantities of ions in its tissues and can yield over 11,000 kg of biomass per hectare[25]. As part of soil salinity reduction practices, *S. europaea* is often harvested at the end of the growing season[26], potentially leaving behind metal ions (e.g., Na^+, K^+, Ca^{2+}) and anions (e.g., CO_3^{2-}, OH^-) in its biomass. We hypothesized that biochar derived from this euhalophyte could exhibit a robust adsorption capacity for cadmium. This is due to these ions facilitating ion exchange or Cd precipitation. Gaining further insight into biochars derived from euhalophytes would not only contribute to the utilization of plant residues but also offer innovative materials for remediating Cd pollution in aquatic environments.

In this study, biochar was generated from the biomass of *Salicornia europaea*. To gain insights into its characteristics, we performed batch adsorption experiments. Our primary objective was to investigate the adsorption behavior of Cd^{2+} ions by the biochar derived from *S. europaea* in aqueous solutions, and subsequently elucidate the underlying adsorption mechanism. To establish a benchmark for comparison, *Zea mays*-derived biochar was employed as a control, as it is widely utilized in the remediation of both aquatic and soil environments.

Materials and methods

Biochar prepared

The *S. europaea* sample was obtained from Karamay city (45° 28′ 6.38″ N, 84° 59′ 41.61″ E), Xinjiang Province, China.The samples were taken to the Laboratory of Fundamental Biology, Xinjiang Institute of Ecology and Geography to be labeled as specimen number 102, and was identified by Dr. Zumei Mao as *Salicornia europaea*. Sample collection has complied with relevant institutional, national, and international guidelines and legislation. The preparation and basic physicochemical properties of *S. europaea*-derived biochar have been mentioned in Ge et al.[22]. The photos of raw and biochar of *S. europaea* are presented in Fig. S1a, b, respectively. The *Z. mays*-derived biochar was purchased from Institute of Soil Science, Chinese Academy of Sciences, Nanjing, China. The biochar derived from *Salicornia europaea* and *Zea mays* were denoted as SBC (*Salicornia europaea*- biochar) and ZBC (*Zea mays*-biochar), respectively.

To remove minerals present in the biochars, as described by Qiu et al.[27] demineralization was carried out by rinsing the biochars with 1 M HCl solution. This was followed by washing with distilled water several times until the pH of the rinsing solution reached a constant value.The demineralized SBC and ZBC were referred to as SBCA and ZBCA, respectively, for further analysis.

Trait analyse

The surface morphology and element distributions of the biochars were analyzed using scanning electron microscopy–energy dispersive X-ray spectroscopy (SEM–EDS) with a Zeiss Supra 55VP instrument (Oregon, USA). The pore structure of the biochars was assessed by N_2 adsorption at 77 K using a Nova 2200e surface area analyzer (Quantachrome Instruments, Florida, USA). The specific surface area (SSA) was calculated using the BET (Brunauer–Emmett–Teller) method, while the average pore volume was determined using the BJH (Barrett-Joyner-Halenda) method.

Zeta potential measurements were performed by dispersing the biochar in solutions ranging from pH 2.0 to 9.0, and the measurements were conducted using a Zetasizer instrument (Nano-ZS90, Malvern, UK). X-ray diffraction was performed using a computer-controlled diffractometer (D8 Advance, Bruker, Germany) with Al-Kα radiation (K-Alpha, Thermo Scientific, USA). Fourier transform infrared spectroscopy (FTIR) was conducted using a Nicolet 6700 instrument (USA) in the wavelength range of 400–4000 cm^{-1}. X-ray photoelectron spectra were acquired using Al-Kα X-rays and a K-Alpha instrument (Thermo Fisher Scientific).

Adsorption capacity measurement

The impact of pH on Cd (II) adsorption by the biochar was investigated within an initial pH range of 2–9. Each adsorbate solution (30 mL) with an initial Cd^{2+} concentration of 30 mg L^{-1} was added to 50 mL polypropylene centrifuge tubes. Subsequently, 20 mg of biochar was introduced to each vial, and the mixtures were allowed to react for 8 h at a temperature of 25 °C ± 0.5 °C.

For the adsorption isothermal experiments, a series of $Cd(NO_3)_2$ solutions ranging from 5 to 100 mg L^{-1} were prepared. The initial pH of the cadmium solution was adjusted to 6.0 ± 0.1 using 0.01 M HNO_3 or NaOH solution to prevent Cd precipitation. Then, 20 mg of biochar and 30 mL of $Cd(NO_3)_2$ solution (5–100 mg L^{-1}) were combined in 50 mL polypropylene centrifuge tubes. The mixtures were shaken at 150 rpm for 8 h at 15, 25 and 35 °C ± 0.5 °C, respectively, followed by centrifugation at 4000 rpm for 10 min. The supernatants were filtered through 0.45 μm filter papers for subsequent Cd concentration analysis.

Regarding the adsorption kinetics experiments, 20 mg of biochar and 30 mL of $Cd(NO_3)_2$ solution (30 mg L^{-1}) were mixed in 50 mL polypropylene centrifuge tubes under the same conditions as the isothermal experiment. The mixtures were treated similarly, and adsorption equilibrium was achieved after shaking. The reaction time was measured at 1, 2, 3, 4, 5, 6, 7, 8, 9, 10, 20, 30, 40, 50, 60, 80, 100, and 120 min, respectively.

All treatments were conducted in quadruplicate. The biochar samples were dried for SEM–EDS, XRD, FTIR, and XPS analyses. The Cd concentration was determined using inductively coupled plasma optical emission spectroscopy (ICP-OES; Agilent 735, USA).

Assessment of Cd^{2+} adsorption mechanisms

The contributions of different mechanisms to Cd^{2+} adsorption on the biochars were determined using a modified version of the method proposed by Wang et al.[9]. The adsorption capacities attributed to metal ion exchange (Q_{CMe}), precipitation with minerals (Q_{CMp}), functional group complexation (Q_{CO}), and Cd^{2+}–π interactions ($Q_{C\pi}$) were determined as follows.

1. In this study, almost no cations (K^+, Na^+, Ca^{2+}, and Mg^{2+}) were observed in the solutions of SBCA and ZBCA (Table S1), implying that adsorption by residual minerals was negligible. Hence, the reduction in the amount of Cd^{2+} sorbed on the biochars after demineralization could be considered as the contribution of these removed minerals[27]. The amount of Cd^{2+} adsorption attributed to the interaction with minerals (Q_{CM}, in mg g^{-1}) was calculated as

$$Q_{CM} = Q_{CT} - Q_{CA} \times Y \tag{1}$$

   where Q_{CT} (mg g^{-1}) is the total adsorption of Cd^{2+} on SBC or ZBC, Q_{CA} (mg g^{-1}) is the amount of sorbed Cd^{2+} on SBCA or ZBCA, and Y is the yield of demineralized biochar from the original biochar.
2. The amount of exchanged base cations (K^+, Ca^{2+}, Na^+, and Mg^{2+}) released from the biochars was determined by the difference in the concentration of these cations in solution before and after Cd^{2+} adsorption. Thus, the amount of Cd^{2+} adsorption resulting from ion exchange (Q_{CMe}) was defined as the sum of exchanged cations:

$$Q_{CMe} = Q_K + Q_{Na} + Q_{Ca} + Q_{Mg} \tag{2}$$

   where Q_K, Q_{Na}, Q_{Ca}, and Q_{Mg} are the net amounts of K, Ca, Na, and Mg released from SBC or ZBC into solution after Cd^{2+} adsorption, respectively. The calculation was normalized to mEq L^{-1}.
3. The adsorption of Cd^{2+} on minerals resulted from a combination of ion exchange and mineral precipitation. Thus, the amount of Cd^{2+} adsorption resulting from mineral precipitation (Q_{CMp}) could be calculated by the difference between Q_{CM} and Q_{CMe}:

$$Q_{CMp} = Q_{CM} - Q_{CMe} \tag{3}$$

4. When the biochars were deashed, the decrease in pH upon Cd^{2+} adsorption on SBCA and ZBCA was attributed to coordination with oxygen-containing organic groups, which can be described by the following reactions[13]:

$$-COOH + Cd^{2+} + H_2O \rightarrow -COOCd^+ + H_3O^+ \tag{4}$$

$$-OH + Cd^{2+} + H_2O \rightarrow -OCd^+ + H_3O^+ \tag{5}$$

The amount of H^+ released was calculated from the decrease in pH, and the amount Cd^{2+} adsorption through functional group complexation (Q_{CO1}) was calculated accordingly. The adsorption attributed to complexation with oxygen-containing functional groups (Q_{CO}) was calculated as

$$Q_{CO} = Q_{CO1} \times Y \tag{6}$$

(5) Cd^{2+} adsorption on SBCA and ZBCA resulted from a combination of Cd^{2+}–π interactions and functional group complexation. Thus, the amount of Cd^{2+} adsorption through Cd^{2+}–π interactions ($Q_{C\pi}$) was calculated by the difference between the Q_{CA} and Q_{CO} values of SBCA and ZBCA:

$$Q_{C\pi} = Q_{CA} \times Y - Q_{CO} \tag{7}$$

In addition, the percentage contributions of the different mechanisms to Cd^{2+} adsorption were calculated as the Q_{CMe}/Q_{CT}, Q_{CMp}/Q_{CT}, Q_{CO}/Q_{CT}, and $Q_{C\pi}/Q_{CT}$ ratios.

Regeneration test

The leaching experiment was carried out to evaluate the stability of biochar for Cd adsorption. The filling height was 30 cm, and inner diameter 5 cm soil column was filled with 10 mg kg^{-1} Cd polluted soil (control group) and 1% SBC, and 2% SBC-amended soil (treated groups), respectively. The following materials were placed in the tube from bottom to top: a layer of filter paper, quartz, a layer of filter paper, 350 g of soil, a layer of filter paper, non-woven fabric. The quartz was washed with 0.01 M NaOH and 0.01 M HCl and dried at 105 °C. Soil density was similar to that of the original soil. Deionized water was poured into the soil columns from the top. Leachate was collected in 50 mL aliquots in a conical flask on 1, 3, 5, 7, 9, 11, 13, 15, 17, 19, 21 days. The leachate was filtered through a 0.45-μm membrane filter for analysis of the heavy metal concentrations.

Statistical analyses

The statistical analyses were performed using SPSS 19.0 (IBM SPSS Inc., Chicago, IL, United States). One-way analysis of variance (ANOVA) was employed to test for significant differences among the treatments. For multiple

comparisons of the mean values, the Tukey test was applied ($P < 0.05$). All the reported results were based on quadruplicate experimental replicates.

Results and discussion

Pore structure and surface charge characterization

The pore structure of biochar plays a significant role in assessing its adsorption efficiency[28]. In this study, the isotherm shapes of the biochars were classified as approximately type IV according to the IUPAC classification system[29]. The SBC exhibited a specific surface area of 6.48 $m^2\ g^{-1}$, which was 56% higher than that of the ZBC (Fig. 1a). This increased specific surface area provides abundant adsorption energy and numerous adsorption sites for Cd^{2+}[30], as the adsorption capacity of biochar is typically proportional to its surface area[31]. Moreover, the SBC displayed a dominant presence of micropores and mesopores, as indicated by the average pore width (4 V A^{-1} based on BET measurements) (Fig. 1b). This pore structure is advantageous for the adsorption of heavy metal cations[32].

The Zeta points of the two biochars under different pH conditions are presented in Fig. S2. As observed, the Zeta point of the biochar decreased with increasing pH value. The surface of the SBC exhibited a negative charge at pH > 2. Compared to the ZBC, the SBC had a smaller zero charge. When the pH of the medium exceeds the point of zero charge (PZC) of the biochar, electrostatic adsorption occurs, allowing for the adsorption of positively charged ions[33].

Solution pH dependent Cd^{2+} adsorption efficiency

The pH value of the solution is a critical parameter that significantly affects the metal adsorption process[34]. In this study, we examined the effect of pH on the removal of Cd by SBC by varying the pH of the solution within the range of 2.0–9.0. As illustrated in Fig. 2, the adsorption efficiency of Cd^{2+} by different biochars increased with the rise in initial solution pH. In the pH range of 2.0–4.0, the adsorption of Cd on SBC exhibited a rapid

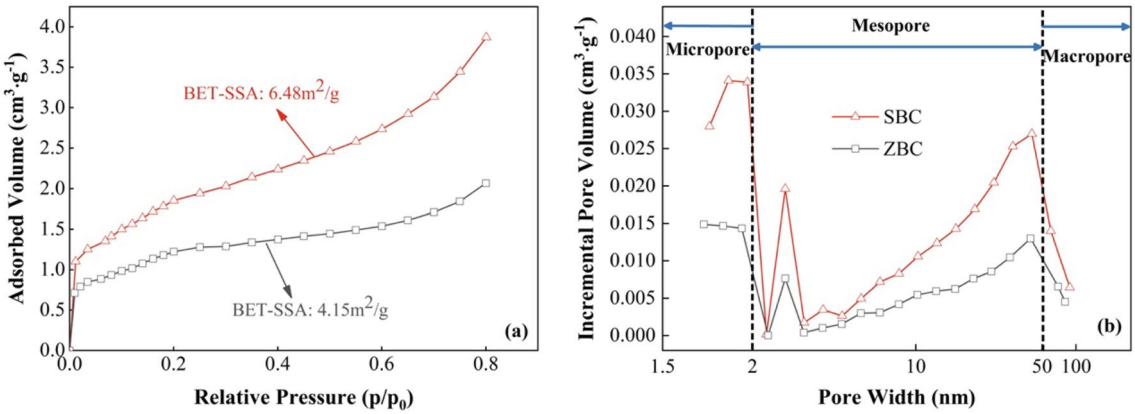


Figure 1. Characterization of the biochar pore structure. (**a**) N_2 adsorption–desorption isotherms and (**b**) corresponding pore size distributions based on the Barrett–Joyner–Halenda (BJH) method. SBC, *Salicornia europaea*- biochar; ZBC, *Zea mays*-biochar.

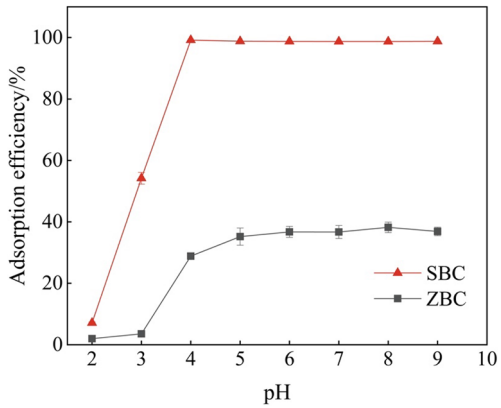


Figure 2. Investigation of pH influence on Cd (II) adsorption by *S. europaea*-biochar (SBC) (**a**) and *Z. mays*-biochar (ZBC) (biochar dosage 20 mg, initial Cd^{2+} concentrations 30 mg L^{-1}, contact time 8 h, temperature 25 °C).

increase, reaching a maximum adsorption efficiency of 99.2% at pH 4 and then remained stable. Conversely, ZBC exhibited the highest adsorption capacity at pH 5.0.

The influence of pH on Cd^{2+} adsorption can be attributed to the surface charge of the adsorbent. When the pH of the solution is below 3.0, the surface of SBC carries a positive charge. This positive charge leads to repulsion, limiting the proximity of Cd^{2+} ions and promoting competition between H^+ and Cd^{2+} for active sites on SBC. Conversely, when the pH exceeds 3.0, the surface of SBC becomes negatively charged, while Cd^{2+} ions are positively charged. As a result, the adsorption is driven by the electrostatic interaction between Cd^{2+} and SBC[35]. Furthermore, as the pH increases, the competition of H^+ for active sites weakens, which explains the enhanced adsorption capacity with higher pH values. Remarkably, even at pH > 7, where the competition of H^+ becomes negligible, SBC still exhibits a strong adsorption capacity, potentially attributed to the precipitation of Cd[36].

The isotherms involved in the Cd^{2+} adsorption

The adsorption capacity of SBC for Cd^{2+} was significantly higher compared to ZBC (Fig. 3). The Langmuir model provided the best fit for the isothermal adsorption curves of SBC (Table 1), indicating that Cd^{2+} adsorption primarily occurred in monolayers with homogeneous active sites on the biochar[37]. The 1/n values ranging from 0.1 to 0.5 for SBC suggested that the main adsorption process took place on its surface[38]. SBC exhibited a maximum adsorption capacity of 108.54 mg g^{-1}, which was 7.4 times higher than that of ZBC (14.69 mg g^{-1}) at 25 °C. The higher ash content in SBC was found to promote the adsorption of Cd[39], which may explain its higher

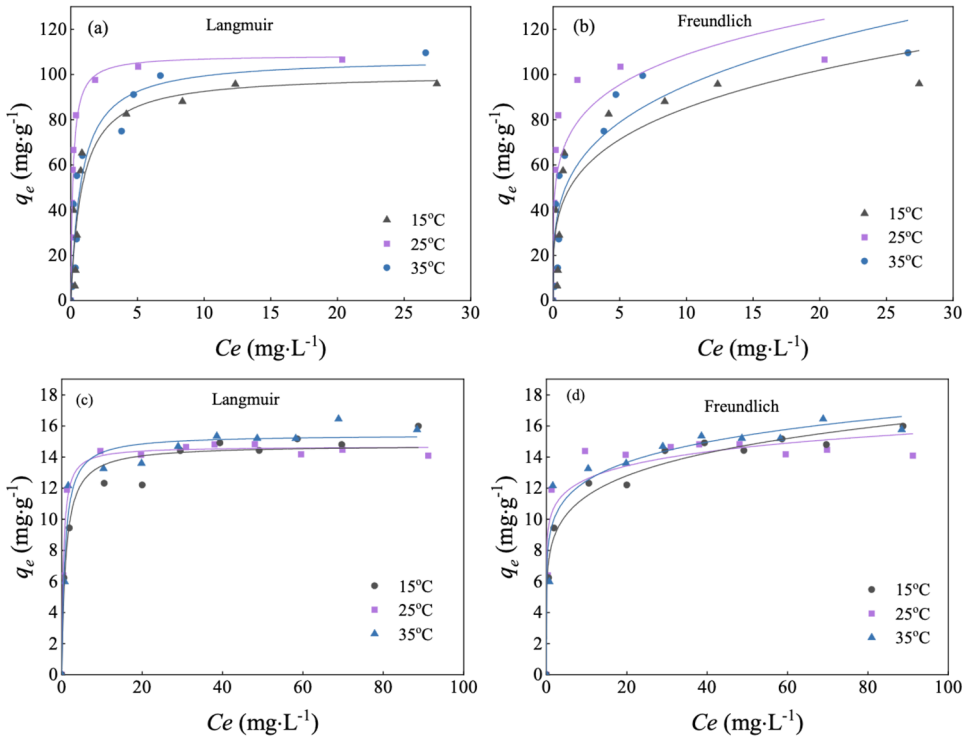


Figure 3. Isothermal adsorption test for Cd^{2+} on *S. europaea*-biochar (SBC) (**a**) and *Z. mays*- biochar (ZBC) (**b**). (Biochar dosage 20 mg, initial Cd^{2+} concentrations ranging from 5 to 100 mg L^{-1}, contact time 8 h, pH 6.0).

Adsorbent	°C	Langmuir parameters			Freundlich parameters			ACPA (mg m^{-2})
		b (L mg^{-1})	q_m (mg g^{-1})	R^2	K_f ($mg^{1-1/n}$ g^{-1} $L^{1/n}$)	1/n	R^2	
SBC	15	1.18	100.28	0.89	47.04	0.26	0.80	16.75
	25	6.04	108.54	0.97	70.42	0.19	0.81	
	35	1.24	107.33	0.90	51.03	0.27	0.84	
ZBC	15	1.01	14.18	0.98	8.01	0.15	0.96	3.54
	25	2.37	14.69	0.99	10.13	0.09	0.92	
	35	1.25	15.44	0.96	9.21	0.13	0.94	

Table 1. Fitting parameters for the Cd adsorption isotherms of *S. europaea* biochar (SBC) and *Z. mays* biochar (ZBC) (biochar dosage 20 mg, initial concentrations of Cd^{2+} 5–100 mg L^{-1}, contact time 8 h, pH 6.0).

adsorption capacity. According to the Langmuir model, the adsorption isotherms of both SBC and ZBC reached a plateau at high Cd concentrations, indicating adsorption saturation.

According to the Langmuir model, both SBC and ZBC exhibited adsorption isotherms reached a plateau at high Cd concentrations, indicating saturation of adsorption. Additionally, the results of thermodynamic parameters showed that the ΔH^0 of SBC was negative, suggesting that the adsorption of Cd^{2+} on SBC is an exothermic process. This could explain the observed lower adsorption capacity of Cd^{2+} by SBC at 35 °C compared to 25 °C (Table 1). In contrast, the ΔH^0 of ZBC was positive, and the adsorption capacity increased with temperature, signifying that the adsorption of Cd^{2+} on ZBC is an endothermic process[40].

The decrease in the R_L value with increasing Cd concentration suggested that higher initial Cd concentrations favored biochar adsorption. Furthermore, the R_L value approaching 0 indicated that Cd adsorption on both biochars was an irreversible process (Fig. S3). Assessing the adsorption efficiency per unit area revealed that SBC had an adsorption efficiency of 16.75 mg m^{-2}, surpassing ZBC, which had an adsorption efficiency of 3.54 mg m^{-2}. By extending the comparison of Cd adsorption capacity to include a broader range of biochars from existing evidence (Table S2), it becomes apparent that SBC was more efficient in sorbing Cd, highlighting its potential for effective Cd remediation.

The kinetics related in the Cd^{2+} adsorption

The adsorption capacity of the biochars for Cd^{2+} initially increased and then reached a plateau, indicating the attainment of equilibrium within 20 min (Fig. S4a). This rapid adsorption in the initial stage suggests that Cd^{2+} predominantly adsorbed onto the outer surfaces of the biochars. Over time, Cd^{2+} gradually diffused into the pores and reacted with internal active sites[41]. The adsorption kinetics of Cd^{2+} on the biochars followed the pseudo-second-order kinetic equation, as evidenced by high R^2 values (> 0.91) and minimal differences between experimental and calculated equilibrium adsorption quantities (Table 2). These findings indicate that Cd adsorption by the biochars was a physiochemically controlled process involving electron sharing or exchange between the biochars and Cd^{2+}[42,43]. Notably, the initial rate of Cd^{2+} adsorption (v_0) was significantly higher for SBC compared to ZBC, indicating a stronger affinity of SBC for Cd^{2+}. Furthermore, the results of Elovich model further revealed that SBC had much higher α values but lower β values than ZBC, suggesting that SBC possesses more active adsorption sites and a stronger electron-donating ability[44].

The adsorption process of Cd^{2+} onto the biochars followed a three-phase mechanism, as observed from the intraparticle diffusion model (Fig. S4b, Table S3). These phases included boundary-layer diffusion (the initial diffusion of Cd^{2+} from the solution onto the biochar surface), intra-particle diffusion (the subsequent mass transfer of Cd^{2+} from the surface into the interior pores of the biochar), and dynamic equilibrium[45]. The findings confirmed the involvement of diffusion in Cd^{2+} adsorption onto the biochars, with pore filling occurring during the adsorption process[46].

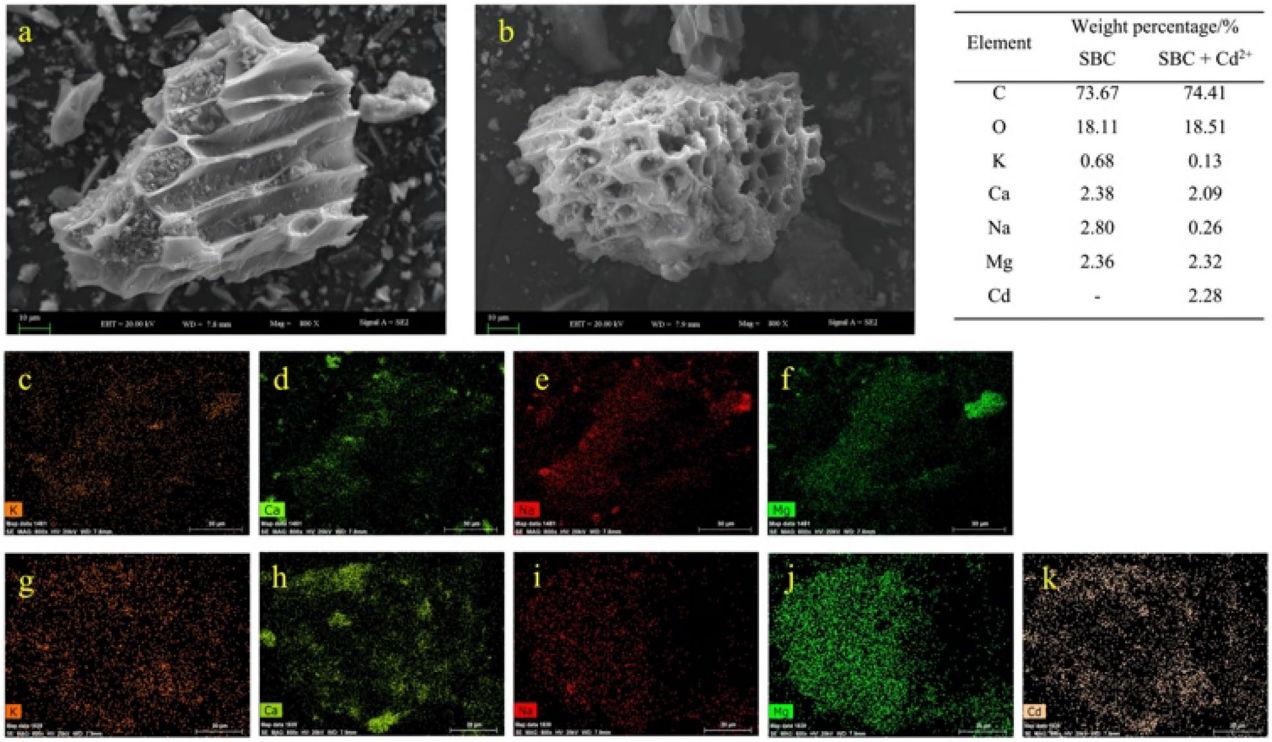
The rate constant (k_{p2}) of SBC was higher than the values reported for other biochars, suggesting a more rapid adsorption process and a shorter adsorption time[47]. This difference could be attributed to the release of salt ions from the porous structure of SBC, thereby increasing the availability of adsorption sites within the pore structure. It is worth noting that the adsorption constant for each adsorption phase was not zero (Table S3), indicating that intraparticle diffusion of Cd^{2+} in the biochar was not the sole process at play. Other mechanisms, such as physical and chemical adsorption on the biochar surface, likely played significant roles, as supported by the pseudo-second-order model and and thermodynamic model. For instance, the values of ΔG^0 in the present study fell within the ranges of − 20 to 0 kJ kJ mol^{-1} (Table S4), indicating a strong physical adsorption[48].

Processes of precipitation with minerals

In this study, the SEM images of the biochars before and after Cd^{2+} adsorption revealed the presence of particles or mineral crystals attached to the biochar surface.. The EDX elemental maps confirmed that these substances were Cd, indicating the formation of Cd-related compounds between Cd and the biochars (Figs. 4, S5).

Kinetic model	Fitting parameter	SBC	ZBC
Pseudo—first order	k_1 (min^{-1})	0.53	0.12
	q_e (mg g^{-1})	40.56	10.73
	R^2	0.87	0.85
Pseudo—second order	k_2 (min^{-1})	0.02	0.01
	q_e (mg g^{-1})	43.08	11.92
	R^2	0.96	0.92
Elovich	α (mg g^{-1} h^{-1})	5070.52	5.70
	β (g mg^{-1})	0.26	0.45
	R^2	0.96	0.96
	v_0 (mg g^{-1} min^{-1})	40.83	1.99

Table 2. Fitting parameters for the kinetics of Cd adsorption on *S. europaea* biochar (SBC) and *Z. mays* biochar (ZBC) (biochar dosage 20 mg, initial concentrations of Cd^{2+} 30 mg L^{-1}, contact time 0–120 min, pH 6.0, temperature 25 °C).



Element	Weight percentage/%	
	SBC	SBC + Cd^{2+}
C	73.67	74.41
O	18.11	18.51
K	0.68	0.13
Ca	2.38	2.09
Na	2.80	0.26
Mg	2.36	2.32
Cd	-	2.28

Figure 4. Scanning electron microscopy–energy dispersive X-ray energy spectroscopy (SEM–EDS) analysis of *S. europaea*- biochar (SBC). SEM images depicting SBC (**a**) and SBC loaded with Cd^{2+} (**b**). Elemental maps derived from EDX analysis showing the distribution of elements in SBC (K: **c**, Ca: **d**, Na: **e**, and Mg: **f**) and SBC loaded with Cd^{2+} (K: **g**, Ca: **h**, Na: **i**, Mg: **j**, and Cd: **k**). The table provides a comprehensive list of elemental contents.

The XRD spectrum of SBC exhibited typical peaks associated with Cd minerals, including $CdCO_3$ and C_2CdO_4 (Fig. 5a). In comparison, ZBC showed a peak of C_2CdO_4 (Fig. S6a). The precipitation of metals through adsorption can be attributed to the alkalinity of the biochars[49]. This mechanism was further confirmed by the variations in CO_3^{2-} concentration in solution before and after Cd^{2+} adsorption (Fig. S7). Specifically, as the initial Cd^{2+} concentration increased, the release of CO_3^{2-} into the solution was significantly reduced for SBC, indicating the involvement of CO_3^{2-} in the Cd^{2+} adsorption process. In contrast, CO_3^{2-} was not detected in the solution of ZBC. Our study demenstrated enhanced adsorption of Cd on SBC can be attributed to the precipitation of Cd with mineral CO_3^{2-} phases of the biochar through complexation. This finding agrees with a previous study that found the formation of cadmium carbonate as a process for the adsorption of cadmium by biochar produced from giant miscanthus[50]. It should be noted that when the temperature exceeded 400 °C, the minerals (mainly $CaCO_3$) present in the mixed biochar obtained by the co-pyrolysis of shrimp shell with corn straw decomposed into CO_2[51]. However, in the case of SBC, a significant amount of CO_3^{2-} was still observed even at 500 °C, indicating that carbonates are more conducive to retention in SBC.

In the XPS spectra, the presence of the Cd 3d peak was detected after Cd^{2+} adsorption on both biochars (Fig. 5b). The forms of Cd included Cd–O,–OCdOH, and $CdCO_3$, with peaks in the range of 405–412 eV[52,53]. These findings suggest that the minerals present in SBC contributed to the adsorption of Cd^{2+}, and Cd^{2+} precipitated in the form of inorganic carbonates or hydroxides.

Processes of metal ion exchange

Some studies have suggested that the contribution of ion exchange to Cd^{2+} adsorption by biochar is negligible[9,54]. However, in our study, we observed a reduction in the weight percentages of K^+, Ca^{2+}, and Na^+ on the biochar surfaces after Cd^{2+} adsorption (Fig. 4). Furthermore, the concentrations of K^+, Ca^{2+}, and Na^+ in the solution increased following Cd adsorption (Fig. S8). By calculating the amount of Cd^{2+} sorbed through metal ion exchange, we found it to be 7.02 mg g^{-1} for SBC. These results indicate that metal ion exchange could be one of the mechanisms through which Cd^{2+} is sorbed onto SBC, in addition to other previously proposed mechanisms.

Processes of surface complexation with oxygen-containing functional groups

The role of inner-sphere surface complexation with oxygen-containing functional groups in Cd^{2+} adsorption was assessed by analyzing the FTIR spectra of the biochars before and after Cd adsorption (Fig. 5c). The original SBC and ZBC biochars exhibited similar functional groups. The main functional groups, including hydroxyl groups (–OH) at 3400 cm^{-1} and carboxyl groups, ketones (C=O) or aromatic components (C=C), and carboxylate

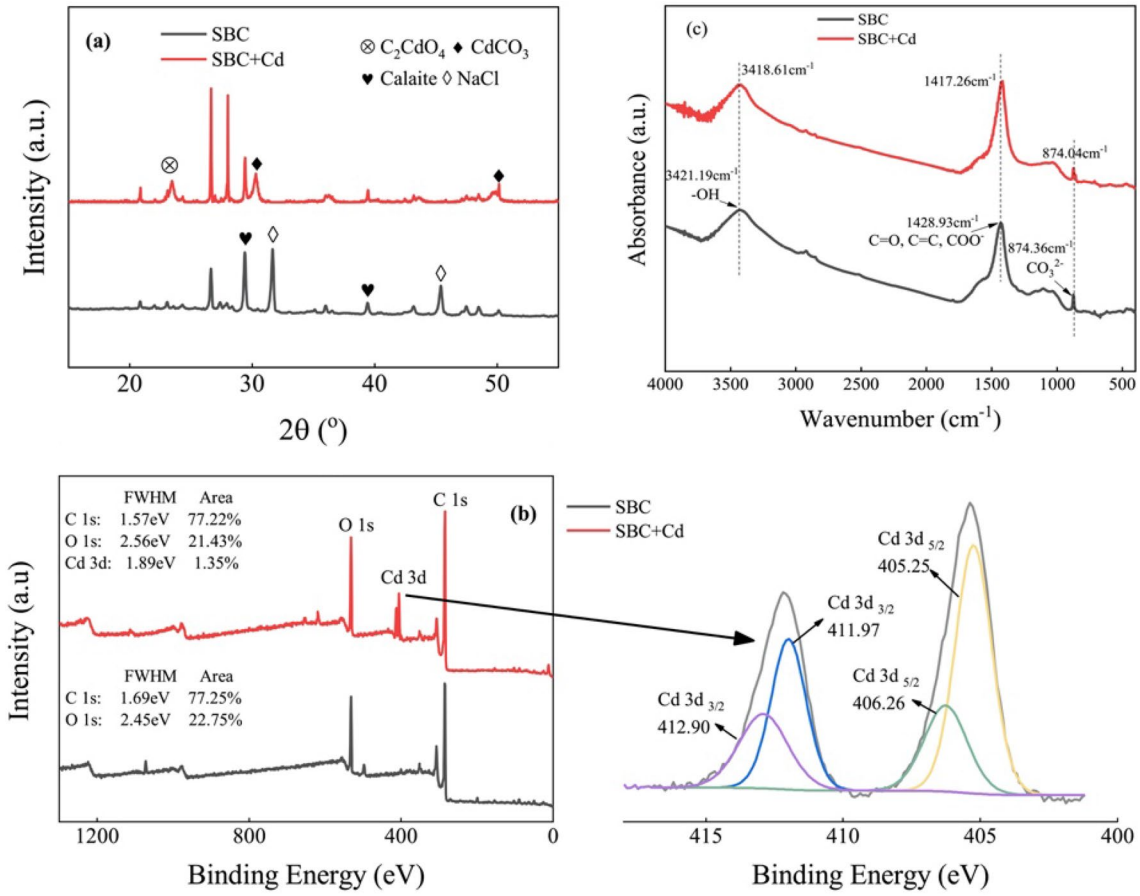


Figure 5. X-ray diffraction patterns (**a**), X-ray photoelectron spectroscopy patterns (**b**), and Fourier transform infrared spectra (**c**) of *S. europaea*-biochar (SBC). The *black* lines represent the original biochar, while the *red* lines depict the biochar loaded with Cd^{2+}.

groups (COO–) in the range of 1380–1700 cm^{-1}, were observed in both biochars. These hydroxyl and carboxyl groups can provide H ions, which are capable of undergoing ion exchange with metal ions[55,56].

In our study, noticeable shifts in the bands at 3400 and 1400 cm^{-1} were observed subsequent to Cd^{2+} adsorption on the biochars, indicating the coordination between –COOH or –OH groups and Cd^{2+}[17]. This coordination process often involves the release of H^+ ions, resulting in a decline in solution pH. To confirm this, we measured the pH values of the solutions before and after Cd^{2+} adsorption by the demineralized SBCA and ZBCA biochars. The pH of the adsorption solutions decreased after Cd^{2+} adsorption on the demineralized biochars, providing further evidence for the complexation of Cd^{2+} with oxygen-containing functional groups on the biochar surfaces.

Processes of Cd^{2+}–π interactions

During pyrolysis process, aromatic structures are formed in biochar, with the cyclic aromatic π-system functions as a π-donor, donating electrons to Cd^{2+} during the adsorption process[57]. To investigate the nature of the adsorption mechanism, we analyzed the C 1s XPS spectra of the biochars before and after Cd^{2+} adsorption, as depicted in Fig. S9. Our analysis revealed the presence of unsaturated structures such as C=O, C–OH, C=C, and π–π* were present on the biochar surfaces. Importantly, the binding energies of aromatic carbonyl carbon (C=O) and hydroxyl carbon (C–OH) exhibited significant changes upon Cd adsorption onto the biochars, providing strong evidence for the involvement of Cd^{2+}–π interactions as a contributing mechanism to the Cd^{2+} adsorption process of SBC.

The contributions from different Cd^{2+} adsorption processes

The contribution of different mechanisms to the total adsorption of Cd^{2+} on both original and demineralised biochar was calculated and presented in Fig. 6. These mechanisms include precipitation with minerals (Q_{CMp}), metal ion exchange (Q_{CMe}), functional group complexation (Q_{CO}), and Cd^{2+}–π interactions ($Q_{C\pi}$) to total Cd^{2+} adsorption (Q_{CT}) on the biochars. The decreasing contributions for both biochars were ranked as follows: $Q_{CMp} > Q_{CMe} > Q_{C\pi} > Q_{CO}$. Only 10% of total Cd^{2+} adsorption on the biochars was attributed to the organic components ($Q_{CO}/Q_{CT} + Q_{C\pi}/Q_{CT}$), while the mineral components (Q_{CM}) accounted for 90% of Cd^{2+} adsorption ($Q_{CMp}/Q_{CT} + Q_{CMe}/Q_{CT}$). Liu et al.[58] also considered that mineral precipitation was the main mechanism of Cd^{2+} adsorption by biochar. It is worth noting that the Q_{CMp} value of SBC was 31.81 mg $Cd^{2+}{\cdot}g^{-1}$, almost five times

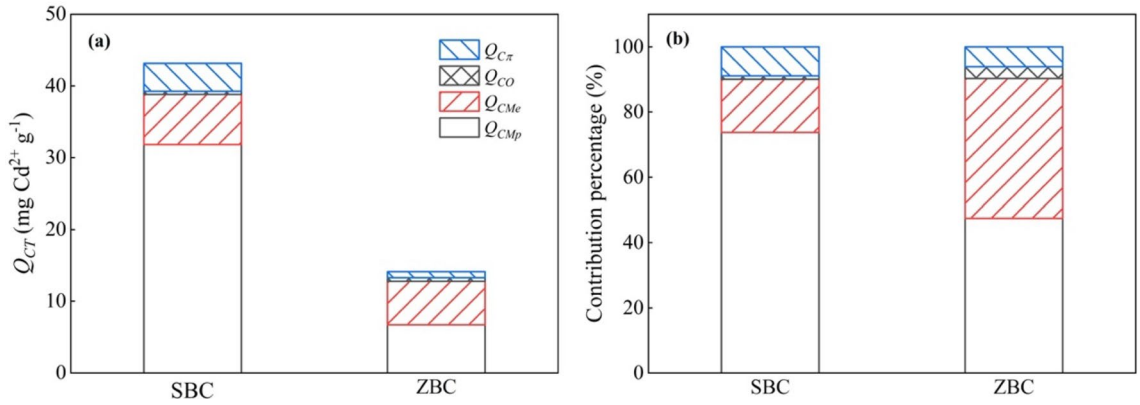


Figure 6. (**a**) Contributions of different mechanisms to Cd^{2+} sorption on *S. europaea* biochar (SBC) and *Z. mays* biochar (ZBC) and (**b**) the contribution percentage of the different mechanisms to overall Cd^{2+} adsorption: precipitation with minerals (Q_{CMp}), metal ion exchange (Q_{CMe}), functional group complexation (Q_{CO}), and Cd^{2+}–π interactions ($Q_{C\pi}$).

higher than that of ZBC. This difference can be attributed to the larger amount of CO_3^{2-} released from SBC into solution before Cd^{2+} adsorption compared to ZBC. In this study, dominant mechanism of Cd^{2+} adsorption on the SBC was found to be the nteraction between minerals and Cd^{2+}.

It is important to note that the physicochemical properties of biochar often undergo changes upon exposure to the environment, as evidenced by numerous studies[59,60]. For instance, as biochar ages, there is an observed increase in surface carboxyl and cation exchange capacity but a decrease in basicity[61]. These alterations may potentially impact its adsorption capacity for Cd. In this study, a short-term leaching test simulating aging revealed that the adsorption capacity of SBC at two concentrations (1% and 2%) did not exhibit a reduction (Fig. S10). However, the adsorption capacity of aged halophyte-biochar is highly expected to decrease beyond a certain threshold. Therefore, the impact of the long-term effects of halophyte-biochar on Cd adsorption certainly requires further evaluation.

Conclusion

The study demonstrated the effective removal of Cd^{2+} from aqueous solution using biochar derived from *S. europaea*. The unique characteristics of this biochar, including its high pH, abundance of base cations, low surface negative charge, and high specific surface area, contributed to its effective adsorption of Cd^{2+}. The study identified multiple mechanisms involved in Cd^{2+} adsorption, including precipitation, metal ion exchange, surface complexation, and Cd^{2+}–π interactions. Among these mechanisms, the surface precipitation of $CdCO_3$ was found to dominate the removal process, highlighting the importance of mineral interactions in Cd adsorption. Overall, this study provides insights into the diverse mechanisms involved in Cd^{2+} adsorption on *S. europaea*-derived biochar. The findings highlight the potential of utilizing biochars derived from euhalophyte plants as effective sorbents for Cd removal in contaminated water systems. Further research in this area can contribute to the development of sustainable and efficient approaches for water remediation and environmental protection.

Data availability

The datasets used and/or analysed during the current study available from the corresponding author on reasonable request.

Received: 3 November 2023; Accepted: 20 December 2023
Published online: 03 January 2024

References

1. Feng, J. *et al.* Enhanced removal performance of zero-valent iron towards heavy metal ions by assembling Fe-tannin coating. *J. Environ. Manage.* **319**, 115619. https://doi.org/10.1016/j.jenvman.2022.115619 (2022).
2. Omidi, F., Behbahani, M., Bojdi, M. K. & Shahtaheri, S. J. Solid phase extraction and trace monitoring of cadmium ions in environmental water and food samples based on modified magnetic nanoporous silica. *J. Magn. Magn Mater.* **395**, 213–220. https://doi.org/10.1016/j.jmmm.2015.07.093 (2015).
3. Sud, D., Mahajan, G. & Kaur, M. P. Agricultural waste material as potential adsorbent for sequestering heavy metal ions from aqueous solutions—a review. *Bioresour. Technol.* **99**, 6017–6027. https://doi.org/10.1016/j.biortech.2007.11.064 (2008).
4. Ge, F., Li, M. M., Ye, H. & Zhao, B. X. Effective removal of heavy metal ions Cd^{2+}, Zn^{2+}, Pb^{2+}, Cu^{2+} from aqueous solution by polymer-modified magnetic nanoparticles. *J. Hazard. Mater.* **211**, 366–372. https://doi.org/10.1016/j.jhazmat.2011.12.013 (2012).
5. Hong, C. Y. *et al.* Effectiveness and mechanism for the simultaneous adsorption of Pb(II), Cd(II) and As(III) by animal-derived biochar/ferrihydrite composite. *Chemosphere* **193**, 133583. https://doi.org/10.1016/j.chemosphere.2022.133583 (2022).
6. Chen, X. *et al.* Adsorption of copper and zinc by biochars produced from pyrolysis of hardwood and corn straw in aqueous solution. *Bioresour. Technol.* **102**, 8877–8884. https://doi.org/10.1016/j.biortech.2011.06.078 (2011).
7. Wang, Z. H. *et al.* Biochar produced from oak sawdust by Lanthanum (La)-involved pyrolysis for adsorption of ammonium (NH_4^+), nitrate (NO_3^-), and phosphate (PO_4^{3-}). *Chemosphere* **119**, 646–653. https://doi.org/10.1016/j.chemosphere.2014.07.084 (2015).

8. Wongrod, S. *et al.* Lead sorption by biochar produced from digestates: Consequences of chemical modification and washing. *J. Environ. Manage.* **219**, 277–284. https://doi.org/10.1016/j.jenvman.2018.04.108 (2018).
9. Wang, Z. *et al.* Investigating the mechanisms of biochar's removal of lead from solution. *Bioresour. Technol.* **177**, 308–317. https://doi.org/10.1016/j.biortech.2014.11.077 (2015).
10. Cui, X. Q. *et al.* Potential mechanisms of cadmium removal from aqueous solution by *Canna indica* derived biochar. *Sci. Total Environ.* **562**, 517–525. https://doi.org/10.1016/j.scitotenv.2016.03.248 (2016).
11. Chen, D. *et al.* The mechanism of cadmium sorption by sulphur-modified wheat straw biochar and its application cadmium-contaminated soil. *Sci. Total Environ.* **714**, 136550. https://doi.org/10.1016/j.scitotenv.2020.136550 (2020).
12. Doumer, M. E., Rigol, A., Vidal, M. & Mangrich, A. S. Removal of Cd, Cu, Pb, and Zn from aqueous solutions by biochars. *Environ. Sci. Pollut. Res.* **23**, 2684–2692. https://doi.org/10.1007/s11356-015-5486-3 (2016).
13. Liu, L. & Fan, S. S. Removal of cadmium in aqueous solution using wheat straw biochar: Effect of minerals and mechanism. *Environ. Sci. Pollut. Res.* **25**, 8688–8700. https://doi.org/10.1007/s11356-017-1189-2 (2018).
14. Dougherty, D. A. Cation-π interactions in chemistry and biology: A new view of benzene, phe, Tyr, and Trp. *Science* **271**, 163–168. https://doi.org/10.1126/science.271.5246.1 (1996).
15. Xu, X. Y., Huang, H., Zhang, Y., Xu, Z. B. & Cao, X. D. Biochar as both electron donor and electron shuttle for the reduction transformation of Cr(VI) during its sorption. *Environ. Pollut.* **244**, 423–430. https://doi.org/10.1016/j.envpol.2018.10.068 (2019).
16. Liu, Y. Y. *et al.* Oxidative ageing of biochar and hydrochar alleviating competitive sorption of Cd(II) and Cu(II). *Sci. Total Environ.* **725**, 138419. https://doi.org/10.1016/j.scitotenv.2020.138419 (2020).
17. Li, B. *et al.* Adsorption of Cd(II) from aqueous solutions by rape straw biochar derived from different modification processes. *Chemosphere* **175**, 332–340. https://doi.org/10.1016/j.chemosphere.2017.02.061 (2017).
18. Han, L. F. *et al.* Removal of antimony (III) and cadmium (II) from aqueous solution using animal manure-derived hydrochars and pyrochars. *Bioresour. Technol.* **234**, 77–85. https://doi.org/10.1016/j.biortech.2017.02.130 (2017).
19. Ahmed, M. B., Zhou, J. L., Ngo, H. H., Guo, W. S. & Chen, M. F. Progress in the preparation and application of modified biochar for improved contaminant removal from water and wastewater. *Bioresour. Technol.* **214**, 836–851. https://doi.org/10.1016/j.biortech.2016.05.057 (2016).
20. Regmi, P. *et al.* Removal of copper and cadmium from aqueous solution using switchgrass biochar produced via hydrothermal carbonization process. *J. Environ. Manage.* **109**, 61–69. https://doi.org/10.1016/j.jenvman.2012.04.047 (2012).
21. Bashir, S., Zhu, J., Fu, Q. L. & Hu, H. Q. Comparing the adsorption mechanism of Cd by rice straw pristine and KOH-modified biochar. *Environ. Sci. Pollut. Res.* **25**, 11875–11883. https://doi.org/10.1007/s11356-018-1292-z (2018).
22. Ge, S. Q. *et al.* Characteristics and acidic soil amelioration effects of biochar derived from a typical halophyte *Salicornia europaea* L. (common glasswort). *Environ. Sci. Pollut. Res.* **30**, 66113–66124. https://doi.org/10.1007/s11356-023-27182-z (2023).
23. Dong, X. L., Wang, J. T., Liu, X. J., Singh, B. & Sun, H. Y. Characterization of halophyte biochar and its effects on water and salt contents in saline soil. *Environ. Sci. Pollut. Res.* **29**, 11831–11842. https://doi.org/10.1007/s11356-021-16526-2 (2022).
24. Alhdad, G. M., Seal, C. E., Al Azzawi, M. J. & Flowers, T. J. The effect of combined salinity and waterlogging on the halophyte *Suaeda maritima*: The role of antioxidants. *Environ. Exp. Bot.* **87**, 120–125. https://doi.org/10.1016/j.envexpbot.2012.10.010 (2013).
25. Cardenas-Perez, S., Piernik, A., Chanona-Perez, J. J., Grigore, M. N. & Perea-Flores, M. J. An overview of the emerging trends of the *Salicornia* L. genus as a sustainable crop. *Environ. Exp. Bot.* **191**, 104606. https://doi.org/10.1016/j.envexpbot.2021.104606 (2021).
26. Zhao, K. F., Song, J., Feng, G., Zhao, M. & Liu, J. P. Species, types, distribution, and economic potential of halophytes in China. *Plant. Soil.* **342**, 495–509. https://doi.org/10.1007/s11104-010-0470-7 (2010).
27. Qiu, Y., Cheng, H., Xu, C. & Sheng, G. D. Surface characteristics of crop-residue-derived black carbon and lead(II) adsorption. *Water Res.* **42**, 567–574. https://doi.org/10.1016/j.watres.2007.07.051 (2008).
28. Hassaan, M. A. *et al.* Isotherm and kinetic investigations of sawdust-based biochar modified by ammonia to remove methylene blue from water. *Sci. Rep.* **13**, 12724. https://doi.org/10.1038/s41598-023-39971-0 (2023).
29. Long, G. L. & Winefordner, J. D. Limit of detection. A closer look at the IUPAC definition. *Anal. Chem.* **55**, 712A-724A. https://doi.org/10.1021/ac00258a001 (1983).
30. Zhang, W. *et al.* Rice waste biochars produced at different pyrolysis temperatures for arsenic and cadmium abatement and detoxification in sediment. *Chemosphere* **250**, 126268. https://doi.org/10.1016/j.chemosphere.2020.126268 (2020).
31. Chen, Z. M., Chen, B. L. & Chiou, C. T. Fast and slow rates of naphthalene sorption to biochars produced at different temperatures. *Environ. Sci. Technol.* **46**, 11104–11111. https://doi.org/10.1021/es302345e (2012).
32. Gao, L. *et al.* Impacts of pyrolysis temperature on lead adsorption by cotton stalk-derived biochar and related mechanisms. *J. Environ. Chem. Eng.* **9**, 105602. https://doi.org/10.1016/j.jece.2021.105602 (2021).
33. Zeng, G. M. *et al.* Enhancement of Cd(II) adsorption by polyacrylic acid modified magnetic mesoporous carbon. *Chem. Eng. J.* **259**, 153–160. https://doi.org/10.1016/j.cej.2014.07.115 (2015).
34. Pehlivan, E., Yanık, B. H., Ahmetli, G. & Pehlivan, M. Equilibrium isotherm studies for the uptake of cadmium and lead ions onto sugar beet pulp. *Bioresour. Technol.* **99**, 3520–3527. https://doi.org/10.1016/j.biortech.2007.07.052 (2008).
35. Houben, D., Evrard, L. & Sonnet, P. Mobility, bioavailability and pH-dependent leaching of cadmium, zinc and lead in a contaminated soil amended with biochar. *Chemosphere* **92**, 1450–1457. https://doi.org/10.1016/j.chemosphere.2013.03.055 (2013).
36. Kolodynska, D. *et al.* Kinetic and adsorptive characterization of biochar in metal ions removal. *Chem. Eng. J.* **197**, 295–305. https://doi.org/10.1016/j.cej.2012.05.025 (2012).
37. Pang, Y. *et al.* PEI-grafted magnetic porous powder for highly effective adsorption of heavy metal ions. *Desalination* **281**, 278–284. https://doi.org/10.1016/j.desal.2011.08.001 (2011).
38. Huang, F., Gao, L. Y., Deng, J. H., Chen, S. H. & Cai, K. Z. Quantitative contribution of Cd^{2+} adsorption mechanisms by chicken-manure-derived biochars. *Environ. Sci. Pollut. Res.* **25**, 28322–28334. https://doi.org/10.1007/s11356-018-2889-y (2018).
39. Zhu, L. *et al.* Key factors and microscopic mechanisms controlling adsorption of cadmium by surface oxidized and aminated biochars. *J. Hazard. Mater.* **382**, 121002. https://doi.org/10.1016/j.jhazmat.2019.121002 (2020).
40. Zhu, X. D. *et al.* Preparation of magnetic porous carbon from waste hydrochar by simultaneous activation and magnetization for tetracycline removal. *Bioresour. Technol.* **154**, 209–214. https://doi.org/10.1016/j.biortech.2013.12.019 (2014).
41. Sun, T. *et al.* Crayfish shell biochar for the mitigation of Pb contaminated water and soil: Characteristics, mechanisms, and applications. *Environ. Pollut.* **271**, 116308. https://doi.org/10.1016/j.envpol.2020.116308 (2021).
42. Vijayaraghavan, K. & Yun, Y. S. Bacterial biosorbents and biosorption. *Biotechnol. Adv.* **26**, 266–291. https://doi.org/10.1016/j.biotechadv.2008.02.002 (2008).
43. Li, X. Y., Gao, X. Y., Ai, L. H. & Jiang, J. Mechanistic insight into the interaction and adsorption of Cr(VI) with zeolitic imidazolate framework-67 microcrystals from aqueous solution. *Chem. Eng. J.* **274**, 238–246. https://doi.org/10.1016/j.cej.2015.03.127 (2015).
44. Chen, Q., Zheng, J. W., Zheng, L. C., Dang, Z. & Zhang, L. J. Classical theory and electron-scale view of exceptional Cd(II) adsorption onto mesoporous cellulose biochar via experimental analysis coupled with DFT calculations. *Chem. Eng. J.* **350**, 1000–1009. https://doi.org/10.1016/j.cej.2018.06.054 (2018).
45. Dos Santos, D. C. *et al.* New carbon composite adsorbents for the removal of textile dyes from aqueous solutions: Kinetic, equilibrium, and thermodynamic studies. *Korean J. Chem. Eng.* **31**, 1470–1479. https://doi.org/10.1007/s11814-014-0086-3 (2014).
46. Liu, Y. *et al.* Enhanced adsorption removal of methyl orange from aqueous solution by nanostructured proton-containing δ-MnO2. *J. Mater. Chem. A* **3**, 5674–5682. https://doi.org/10.1039/C4TA07112C (2015).

47. Cheng, H. *et al*. Hierarchical porous biochars with controlled pore structures derived from co-pyrolysis of potassium/calcium carbonate with cotton straw for efficient sorption of diethyl phthalate from aqueous solution. *Bioresour. Technol.* **346**, 126604. https://doi.org/10.1016/j.biortech.2021.126604 (2022).
48. Feng, Y. *et al*. Basic dye adsorption onto an agro-based waste material—Sesame hull (*Sesamum indicum* L.). *Bioresour. Technol.* **102**, 10280–10285. https://doi.org/10.1016/j.biortech.2011.08.090 (2011).
49. Xu, X. Y. *et al*. Removal of Cu, Zn, and Cd from aqueous solutions by the dairy manure-derived biochar. *Environ. Sci. Pollut. R.* **20**, 358–368. https://doi.org/10.1007/s11356-012-0873-5 (2013).
50. Kim, W. K. *et al*. Characterization of cadmium removal from aqueous solution by biochar produced from a giant Miscanthus at different pyrolytic temperatures. *Bioresour. Technol.* **138**, 266–270. https://doi.org/10.1016/j.biortech.2013.03.186 (2013).
51. Liu, J., Yang, X. Y., Liu, H. H., Jia, X. P. & Bao, Y. C. Mixed biochar obtained by the co-pyrolysis of shrimp shell with corn straw: Co-pyrolysis characteristics and its adsorption capability. *Chemosphere* **282**, 131116. https://doi.org/10.1016/j.chemosphere.2021.131116 (2021).
52. Huang, Q. Q. *et al*. Magnetic graphene oxide/MgAl-layered double hydroxide nanocomposite: One-pot solvothermal synthesis, adsorption performance and mechanisms for Pb^{2+}, Cd^{2+}, and Cu^{2+}. *Chem. Eng. J.* **341**, 1–9. https://doi.org/10.1016/j.cej.2018.01.156 (2018).
53. Cui, L. Q. *et al*. Physicochemical disintegration of biochar: A potentially important process for long-term cadmium and lead sorption. *Biochar* **3**, 511–518. https://doi.org/10.1007/s42773-021-00108-z (2021).
54. Li, M. *et al*. Cu(II) removal from aqueous solution by *Spartina alterniflora* derived biochar. *Bioresour. Technol.* **141**, 83–88. https://doi.org/10.1016/j.biortech.2012.12.096 (2013).
55. Fan, J. J. *et al*. Remediation of cadmium and lead polluted soil using thiol-modified biochar. *J. Hazard. Mater.* **388**, 122037. https://doi.org/10.1016/j.biortech.2012.12.096 (2020).
56. Shetty, R., Vidya, C. S. N., Prakash, N. B., Lux, A. & Vaculik, M. Aluminum toxicity in plants and its possible mitigation in acid soils by biochar: A review. *Sci. Total Environ.* **765**, 142744. https://doi.org/10.1016/j.scitotenv.2020.142744 (2021).
57. Park, J. H., Wang, J. J., Zhou, B. Y., Mikhael, J. E. R. & DeLaune, R. D. Removing mercury from aqueous solution using sulfurized biochar and associated mechanisms. *Environ. Pollut.* **244**, 627–635. https://doi.org/10.1016/j.envpol.2018.10.069 (2019).
58. Liu, X. Y. *et al*. Banana stem and leaf biochar as an effective adsorbent for cadmium and lead in aqueous solution. *Sci. Rep.* **12**, 1584. https://doi.org/10.1038/s41598-022-05652-7 (2022).
59. Nan, Q., Hu, S. L., Qin, Y. & Wu, W. X. Methane oxidation activity inhibition via high amount aged biochar application in paddy soil. *Sci. Total Environ.* **796**, 149050. https://doi.org/10.1016/j.scitotenv.2021.149050 (2021).
60. Cui, H. B. *et al*. Aging reduces the bioavailability of copper and cadmium in soil immobilized by biochars with various concentrations of endogenous metals. *Sci. Total Environ.* **797**, 149136. https://doi.org/10.1016/j.scitotenv.2021.149050 (2021).
61. Wang, H. *et al*. Effects of atmospheric ageing under different temperatures on surface properties of sludge-derived biochar and metal/metalloid stabilization. *Chemosphere* **184**, 176–184. https://doi.org/10.1016/j.chemosphere.2017.05.175 (2017).

Acknowledgements

This work was supported by the National Natural Science Foundation of China (grant no. 31971448), the National Key Research and Development Program of China (grant no. 2022YFD1900101), the Foundation of Science & Technology Department of Xinjiang Uygur Autonomous Region (grant no. 2019XS28) and the Youth Innovation Promotion Association CAS (grant no. 2020433). We thank the editor and reviewers for their constructive suggestions and insightful comments.

Author contributions

S.G., S.Q. wrote the main manuscript text, Wang, L. Z., Z.Y. and W.S.L. prepared figures, Z.S. and T.C.Y. provided the Funding and reviewed the manuscript text. All authors reviewed the manuscript.

Competing interests

The authors declare no competing interests.

Additional information

Supplementary Information The online version contains supplementary material available at https://doi.org/10.1038/s41598-023-50525-2.

Correspondence and requests for materials should be addressed to S.Z. or C.T.

Reprints and permissions information is available at www.nature.com/reprints.

Publisher's note Springer Nature remains neutral with regard to jurisdictional claims in published maps and institutional affiliations.

Open Access This article is licensed under a Creative Commons Attribution 4.0 International License, which permits use, sharing, adaptation, distribution and reproduction in any medium or format, as long as you give appropriate credit to the original author(s) and the source, provide a link to the Creative Commons licence, and indicate if changes were made. The images or other third party material in this article are included in the article's Creative Commons licence, unless indicated otherwise in a credit line to the material. If material is not included in the article's Creative Commons licence and your intended use is not permitted by statutory regulation or exceeds the permitted use, you will need to obtain permission directly from the copyright holder. To view a copy of this licence, visit http://creativecommons.org/licenses/by/4.0/.

© The Author(s) 2024